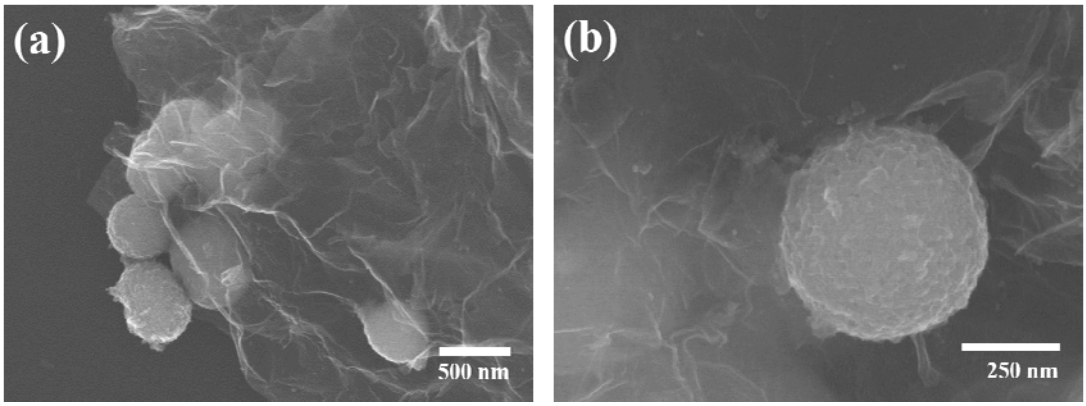

Figure S1. (a), (b) FESEM images of ZnS-NiS_2-G (5%)

Figure S1 (a), (b) show the morphology of ZnS-NiS_2-G (5%). In **Figure S1** (a), there are numerous folded nanosheets, which are graphene nanosheets. Some of the ZnS-NiS_2 nanospheres are fixed on the surface of graphene, while others are wrapped and covered by graphene nanosheets. Graphene nanosheets can link the sulfide nanospheres together, expanding the contact area with electrolytes and providing more redox reaction sites.

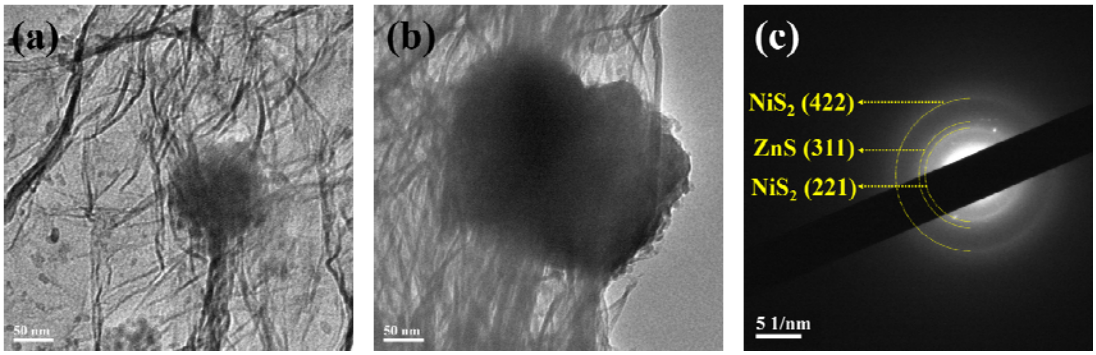

Figure S2. (a), (b) TEM images of ZnS-NiS_2-G (5%), (c) SAED image of ZnS-NiS_2-G (5%)

Figure S2 (a), (b) show the TEM images of ZnS-NiS_2-G (5%). The ZnS-NiS_2-G (5%) sample have a morphology of ZnS-NiS_2 covered by graphene nanosheets. The black lines in TEM images may be fold structure of graphene. **Figure S2** (c) shows the SAED image of the ZnS-NiS_2-G (5%) sample. Diffraction rings are corresponded with the (422), (221) crystal planes of NiS_2 and the (311) crystal planes of ZnS respectively. However, there is no diffraction ring that is matched with graphene. This may be caused by relatively low content of graphene, and the relatively low diffraction signal yield of graphene.

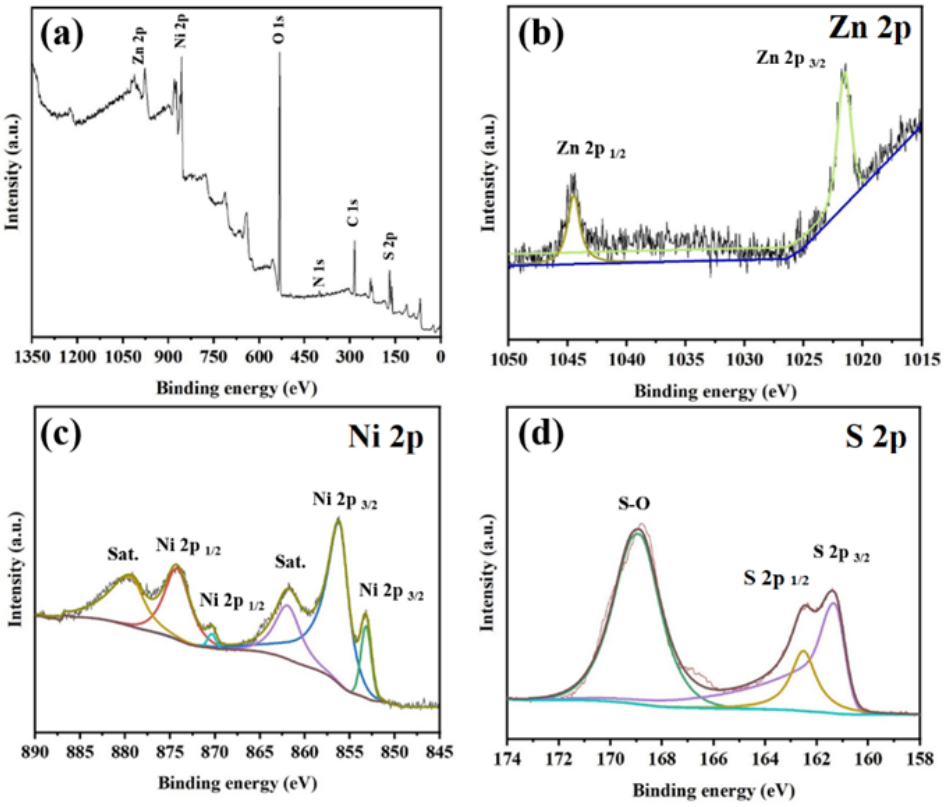

Figure S3. (a) XPS spectrum of ZnS-NiS_2-1:7 sample, (b), (c), (d) high-resolution spectra of Zn, Ni, and S element regions.

The provided data in **Figure S3 (a)** depicts the XPS full spectrum of the ZnS-NiS_2-1:7 sample, revealing the peaks of Zn, Ni, O, N, C, and S elements. Notably, a common peak in the XPS full spectrum is due to the adsorption of air components during the testing process. In **Figure S3 (b)**, a high-resolution spectrum of the Zn element is depicted, with the overall background noise being more obvious. This may be due to the low ZnS composite ratio in the ZnS-NiS_2-1:7 sample, resulting in a small Zn element mass on the sample surface. Furthermore, **Figure S3(c)** is the high-resolution spectrum of the Ni element, where the peaks at 874.2 eV and 856.4 eV correspond to the $2p_{1/2}$ and $2p_{3/2}$ orbitals of Ni^{3+}. Additionally, the peaks at 879.7 eV and 861.9 eV are satellite peaks of Ni^{3+} and Ni^{2+}, respectively, indicating the coexistence of trivalent and divalent Ni elements, suggesting surface oxidation. Moreover, **Figure S3 (d)** is a high-resolution spectrum of the S element. The two peaks at 162.5 eV and 161.4 eV correspond to the $2p_{1/2}$ and $2p_{3/2}$ orbitals, and the peak at 168.9 eV suggests the presence of S-O bonds. The existence of S-O bonds indicates that the surface components of the sample have been oxidized, consistent with the existence of Ni^{3+}. It may be due to the oxidation of metal sulfides on the surface that occurred during the storage process of the sample, leading to the formation of metal sulfides.

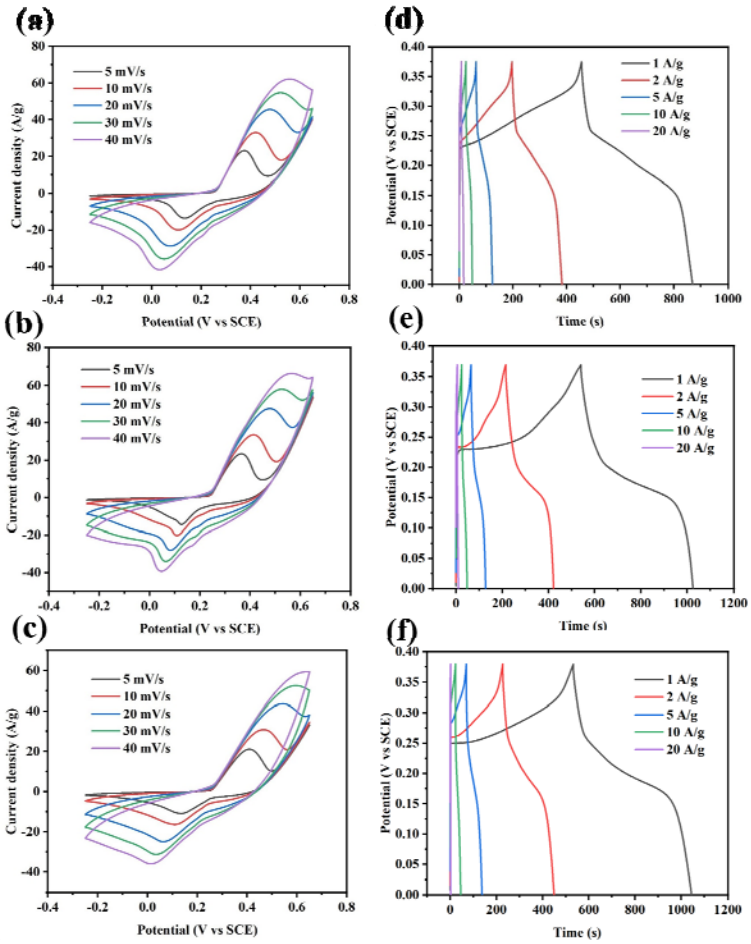

Figure S4. (a), (b), (c) CV curves of ZnS-NiS_2-0:1, 1:9, 1:5 samples, (d), (e), (f) GCD curves of ZnS-NiS_2-0:1, 1:9, 1:5 samples.

Figure S4 shows the CV and GCD curves of the ZnS-NiS_2-0:1, 1:9, 1:5 samples. There is a pair of redox peaks in all CV curves and platform areas in all GCD curves, proving that the ZnS-NiS_2-0:1, 1:9, 1:5 samples are pseudocapacitive materials. Specific capacitance of the ZnS-NiS_2-0:1, 1:9, 1:5 samples was calculated to be 1164.3, 1326.9, 1364.0 F g^{-1} at 1 A g^{-1} respectively.

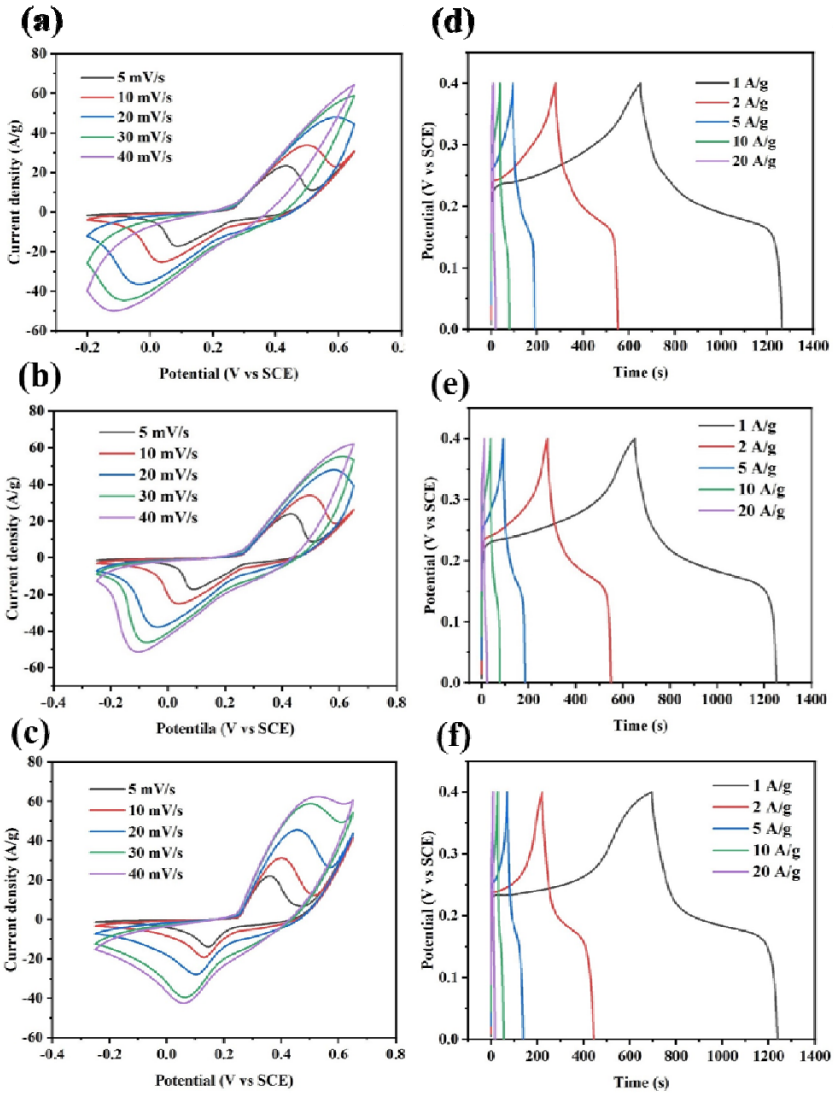

Figure S5. (a), (b), (c). CV curves of ZnS-NiS_2-G (3%, 7%, 9%) electrodes, (d), (e), (f) GCD curves of ZnS-NiS_2-G (3%, 7%, 9%) electrodes.

Figure S5 shows the electrochemical performance of ZnS-NiS_2-G (3%, 7%, 9%) samples. There is a pair of redox peaks in all CV curves and platform areas in all GCD curves. It indicates that the addition of graphene nanosheets will not change pseudocapacitive behavior or the ZnS-NiS_2-1:7. Specific capacitance of the ZnS-NiS_2-G (3%, 7%, 9%) samples was calculated to be 1566.7, 1528.8, 1401.1 F g^{-1} at 1 A g^{-1} respectively.

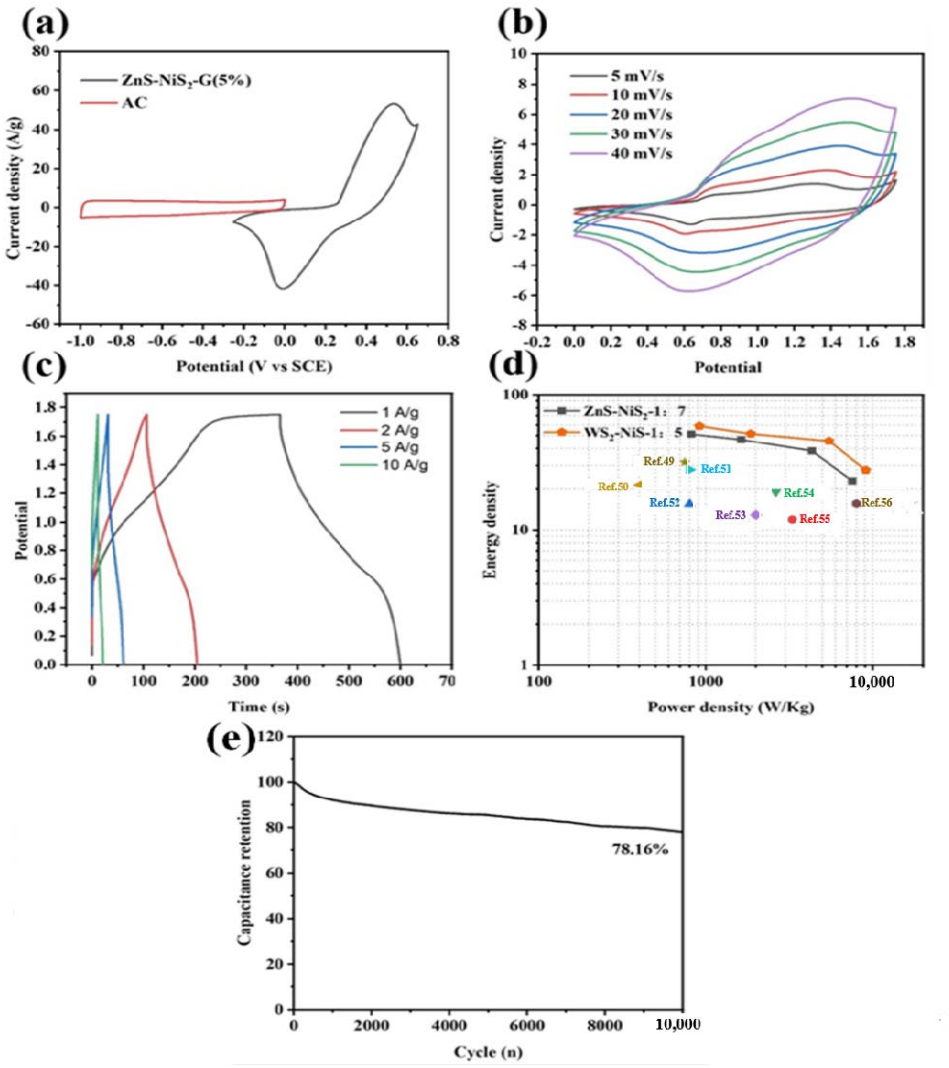

Figure S6 (a) CV graphs of ZnS-NiS2-G (5%) and AC electrode, (b) CV curve of ZnS-NiS2-G (5%)//AC device, (c) GCD curve of ZnS-NiS2-G (5%)//AC device, (d) comparison of ragone diagram of ZnS-NiS2-G (5%) and ZnS-NiS2-1:7 devices [49-56] (e) cyclic stability of ZnS-NiS2-G(5%)//AC device.

Figure S6 (a) shows the CV curves of the ZnS-NiS2-G(5%) positive electrode and the AC negative electrode. In **Figure S6 (b)**, the CV diagram of the ZnS-NiS2-G(5%)//AC device illustrates consistent CV curve shapes as the scan speed increases, indicating good reversibility and fast charge and discharge capabilities. **Figure S6(c)** shows the GCD curve of the ZnS-NiS2-G(5%)//AC device is approximately triangular, indicating the existence of double-layer capacitance and pseudocapacitance behavior during the energy storage process of the device. Additionally, the cycling stability of the ZnS-NiS2-G(5%)//AC device at 10 A g^{-1} is shown in the **Figure S6 (f)**. After 10,000 cycles, the retention of 78.16% of the specific capacitance indicates good cycle stability. The addition of graphene, however, has resulted in a slight reduction in cyclicity. This may be due to the physical compounding method, especially ultrasonic and magnetic stirring, which may hinder the formation of a chemical

bond between graphene and sulfide. As a result, the combination between the two materials may not be strong enough, leading to the detachment or structural damage of some electrode materials during the charge and discharge cycles, consequently diminishing the cycle performance. In the near future, we are interested in performing cycle stability experiments on the three-electrode system and determining the coulombic efficiency of both the three-electrode and two-electrode configurations.